Journal of Alloys and Compounds 650 (2015) 482–488

Contents lists available at ScienceDirect

Journal of Alloys and Compounds

journal homepage: http://www.elsevier.com/locate/jalcom

Developing magnetofunctionality: Coupled structural and magnetic phase transition in $AlFe_2B_2$

L.H. Lewis [a, b, c, *], R. Barua [a, b, c], B. Lejeune [a, c]

[a] Department of Chemical Engineering, Northeastern University, Boston, MA 02115, USA
[b] Department of Mechanical and Industrial Engineering, Northeastern University, Boston, MA 02115, USA
[c] George J. Kostas Research Institute for Homeland Security, Northeastern University, Burlington, MA, USA

ARTICLE INFO

Article history:
Received 18 June 2015
Received in revised form
24 July 2015
Accepted 27 July 2015
Available online 30 July 2015

Keywords:
AlFe2B2
Magnetostructural
Magnetocaloric
Structure-property correlations

ABSTRACT

Understanding correlations between crystal structure and magnetism is key to tuning the response of magnetic materials systems that exhibit large functional effects in response to small excursions in magnetic field or strain. To this end, temperature-dependent structure-magnetic property correlations are reported in samples of $AlFe_2B_2$ with the orthorhombic $AlMn_2B_2$-type layered structure as it traverses a thermally-hysteretic first-order magnetic phase change at a transition temperature of $T_t = 280$ K. Temperature-dependent x-ray diffraction carried out in the temperature range 200 K $\leq T \leq$ 298 K reveals that the *a* and *b* lattice parameters increase by 0.2% and 0.1% respectively upon heating, while the *c* lattice parameter decreases by 0.3%, providing a conserved unit cell volume through T_t. A very small volumetric thermal expansion coefficient 4.4×10^{-6}/K is determined in this temperature range that is one order of magnitude smaller than that of aluminum and only slightly larger than that of Invar. The latent heat of transformation associated with this magnetostructural phase transformation is determined as 4.4 J/g, similar to that of other magnetostructural materials. Overall, these features confirm a first-order thermodynamic phase change in the $AlFe_2B_2$ system that emphasizes strong coupling between the magnetic spins and the lattice to support potential magnetofunctional applications for energy transformation and harvesting.

1. Introduction

Efficient thermal management, an important component of energy sustainability, may be addressed by systems and devices that feature multifunctional materials. Thermal management in air conditioning and refrigeration systems is highly energy intensive: 15% of the world's electric power is devoted to cooling, with that value increasing to 20% in the U.S. and to 25% in Japan [1]. Further, there are other significant detriments associated with current vapor-compression cooling technology such as significant carbon emissions and environmentally-damaging leaks of chemical refrigerant [1]. In parallel, there is much ambient thermal energy that, if captured, can be re-introduced into energy conversion systems. Generation of such dissipated "waste heat" occurs in microelectronic devices, vehicles and large-scale industrial process plants, to name but a few sources. Indeed, a study conducted by Lawrence Berkeley National Laboratory estimated that in 2011 the United States possessed 100 GW of untapped electrical capacity in the form of waste heat that annually could produce 742 TW-hr of power [2]. It is clear that successful realization of energy-efficient and green cooling technologies, combined with distributed thermal energy harvesting, will help address the global energy challenge.

One class of multifunctional materials appropriate for thermal management applications are those that exhibit significant caloric effects [3]. So-called "caloric" materials experience temperature changes under isothermal or adiabatic variations of a control field (of electric, strain and/or magnetic in nature) [3]. The magnetocaloric effect, triggered by the cyclic application and removal of a magnetic field, can be large in materials with very strong coupling between crystallographic and the magnetic lattices [4]. In such materials, referred to as magnetostructural materials, the application of a magnetic field induces simultaneous changes of magnetic and lattice entropies that may then be transformed into thermal energy changes [4]. There are a number of active magnetocaloric

* Corresponding author. Department of Chemical Engineering, Northeastern University, Boston, MA 02115, USA.
E-mail addresses: lhlewis@neu.edu (L.H. Lewis), radhika.barua@gmail.com (R. Barua).

http://dx.doi.org/10.1016/j.jallcom.2015.07.255
0925-8388/

refrigeration and thermal energy harvesting device designs in existence today that are anticipated to provide highly efficient energy transformations, provided that appropriate magnetofunctional working materials may be developed [5]. This materials challenge has proven to be formidable; in addition to difficulties with materials fabrication, mechanical integrity and corrosion issues during cycling, many magnetothermal materials under consideration today contain rare, toxic or strategically-limited elements: these materials include Gd, $Gd_5(GeSi)_4$, FeRh, MnAs, FeMnAsP and $(La((FeCo)Si(H))_{13}$ [4–7]. Against this backdrop the recent report of a room-temperature magnetocaloric effect in the ferromagnetic compound $AlFe_2B_2$ is of interest [8]. This intermetallic compound is comprised entirely of non-critical, easily accessible, stable and easily recyclable elements. Reports to date briefly describe the magnetic phase transition found in $AlFe_2B_2$ but provide no data or insight concerning lattice–magnetism interactions as material traverses the magnetic phase transition; such information is crucial to understanding fundamental and applied phenomena in this compound. To this end, magnetic, structural and calorimetric data indicate that the ferromagnetic (FM) → paramagnetic (PM) phase transformation of $AlFe_2B_2$ crystallites is a magnetostructural transformation of first-order thermodynamic character, confirming the existence of very strong coupling between the magnetic and crystallographic lattices. Significantly, while the lattice parameters of the orthorhombic $AlMn_2B_2$-type unit cell of $AlFe_2B_2$ are temperature dependent, the unit cell volume changes very little through the magnetic phase transition. These results are important for understanding and tailoring the magnetofunctional response of the novel $AlFe_2B_2$ material, of potential interest for magnetic cooling and magnetothermal-based energy harvesting applications [4,7,9,10].

At room temperature $AlFe_2B_2$ adopts a layered orthorhombic $AlMn_2B_2$-type crystal structure (space group *Cmmm*), as first reported by Jeitschko in 1969 [11,12]. This structure, shown in Fig. 1, consists of two formula units with Fe and B atoms forming a Fe_2B_2 layer within the (*ac*) plane that are separated by a monolayer of Al atoms arranged along the orthorhombic *b*-axis (Fig. 1(a)). The Fe and B atoms of each formula unit are located at the fractional coordinate sites *4j* (0, 0.35, 0.5) and *4i* (0, 0.21, 0), respectively, such that each Fe atom is covalently bonded to four B atoms in the (*ac*) plane and to a further two B atoms in the (*bc*) plane. The B atoms form zig-zag chains down the length of the *a*-axis, adjacent to one another along the *c*-axis [8,11]. When viewed in the (*ac*)-plane, the Fe_2B_2 chains form a wavy layer (Fig. 1(c)), with Fe atoms located between parallel layers of B atoms such that each Fe atom forms six Fe–B bonds. As a relatively new compound, $AlFe_2B_2$ is largely unexplored. To date, only a handful of 1-2-2 intermetallic compounds have been reported to crystallize in the $AlMn_2B_2$-type structure: these are AlT_2B_2 (T = Cr, Mn, Fe), PbR_2Ni_2 (R = rare earth element) and $CdGd_2Ni_2$ [11–15]. At room temperature, $AlFe_2B_2$ is reported to demonstrate itinerant ferromagnetism with a saturation magnetization (M_s) of ~1 μ_B per Fe atom at $T = 4.2$ K [16]. Upon heating, a ferromagnetic (FM) → paramagnetic (PM) phase transformation is observed at a transition temperature of 320 K [16]. In 2013 Tan et al. reported an isothermal magnetic entropy change (ΔS_{mag}) of 4.1 J $kg^{-1}K^{-1}$ at an applied field of 2 T and calculated a temperature change (ΔT_{ad}) of 2 K using measured magnetic data [8]. The room temperature zero-field heat capacity of $AlFe_2B_2$ was determined as 110 J/mole K [8]. Building on the results of Tan et al., Chai et al. investigated ternary compounds of AlT_2B_2 (T = Mn, Cr) and found that $AlMn_2B_2$ and $AlCr_2B_2$ are predominantly paramagnetic in character in the temperature range of 1.8–400 K [12]. Further, room-temperature examination of quaternary compounds of composition $AlFe_{2-x}Mn_xB_2$ ($0 \leq x \leq 1.0$) indicates that substitution of Mn for Fe in the $AlFe_2B_2$ lattice increases the unit cell volume but suppresses the ferromagnetism [13].

2. Experimental methods

Bulk $AlFe_2B_2$ was synthesized by arc melting the constituent elements (99.9% purity) in a 1.5 Al: 2 Fe: 2 B M ratio. Excess Al was intentionally added to the arc-melted samples to maximize the

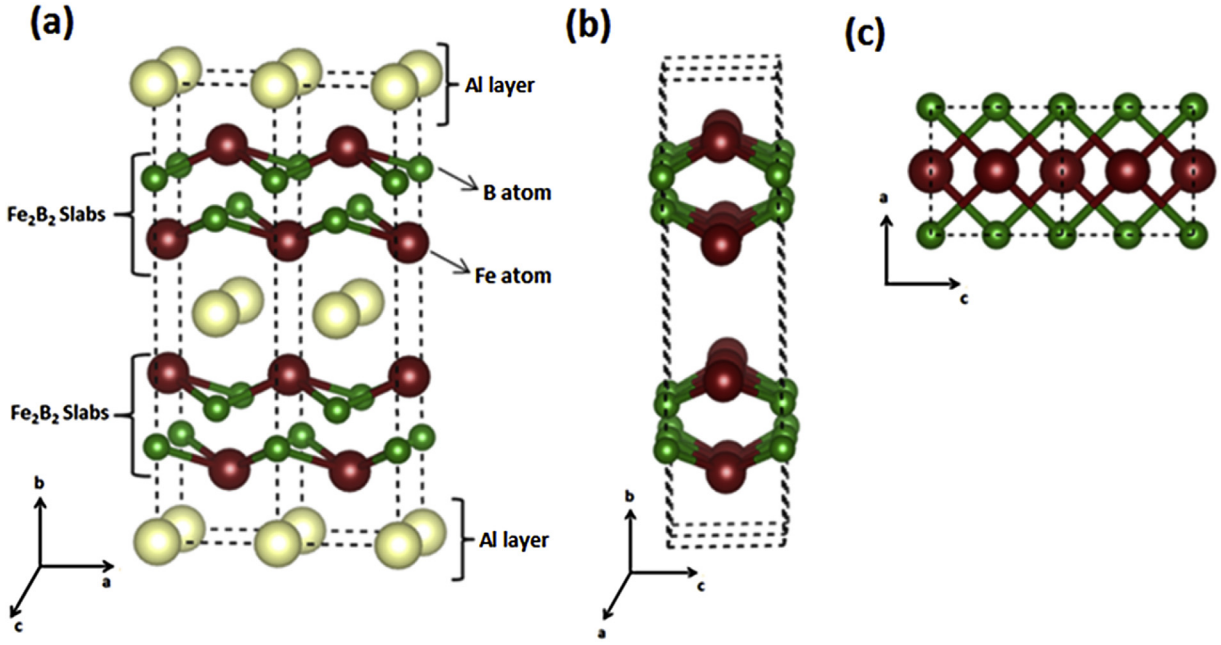

Fig. 1. Layered orthorhombic crystal structure of $AlFe_2B_2$ from the perspective of the (*ab*), (*ac*) and (*bc*) planes: (a) Each unit cell consists of two formula units with Fe and B atoms forming a Fe_2B_2 layer within the (*ac*) plane that are separated by a monolayer of Al atoms arranged along the orthorhombic *b*-axis; (b) The Fe and B atoms in the Fe_2B_2 chains are located such that each Fe atom is covalently bonded to four B atoms in the (*ac*) plane and to a further two B atoms in the (*bc*) plane; (c) In the (*ac*)-plane, the Fe_2B_2 chains form a wavy layer with Fe atoms located between parallel layers of B atoms.

$AlFe_2B_2$ phase content [8]. The arc-melted charges were sliced into slabs of 1 mm thickness x 3 mm width x 5 mm length, mass ~25 mg, using a low-speed diamond saw and metallographically polished to a mirror finish. Polished slices were then sealed under vacuum (1×10^{-6} Torr) in vitreous silica tubes and annealed at 1000 °C for 14 days. All subsequent characterization was performed on the samples in this above-described slice form.

Structural, magnetic and calorimetric attributes of the $AlFe_2B_2$ sample were characterized using several probes. Microstructural observation was carried out using optical and scanning electron microscopy (SEM, Hitachi S4800). The chemical composition of each phase within the sample was determined using SEM energy-dispersive x-ray spectrometry (EDS). The crystal structure of $AlFe_2B_2$ was examined with Cu-K_α X-ray diffraction (XRD, PAN-analytical X'Pert PRO) at room temperature in the range $10° \leq 2\theta \leq 80°$ and at lower temperatures 200 K ≤ T ≤ 298 K in the range $30° \leq 2\theta \leq 55°$. Data were collected upon cooling from room temperature to 200 K. The smaller 2θ range was employed during temperature-dependent XRD examination to optimize the available data collection time. For low-temperature XRD measurements the sample was sealed in a cryostat-cooled chamber (Oxford PheniX) mounted on a stage that automatically adjusted for thermal contraction. The data were calibrated using crystalline Si powder combined with the sample. Bragg reflections obtained from the x-ray diffraction patterns were fit with a pseudo-Voight function and successfully indexed to an orthorhombic unit cell. Lattice parameters were determined using a least squares method [17]. Based on the least squares fit of the room-temperature XRD data, the accuracy of the lattice parameters calculated from the temperature-dependent XRD scans is determined to be on the order of ±0.005 Å.

Magnetic characterization was carried out using a Vibrating Sample Magnetometer (Quantum Design model VersaLab) in magnetic fields up to $\mu_0 H_{app} = 3$ T and in the temperature range 50 K ≤ T ≤ 390 K. The field was applied in-plane and no demagnetization corrections were applied. The temperature sweep-rate for all temperature-dependent magnetic measurements was set at 10 K/min. The magnetic transition temperature T_t was determined as the inflection point in the derivative of magnetization M as a function of temperature T at an applied field of 0.1 T. The magnitude of the magnetothermal hysteresis in the samples was determined as the difference between temperature inflection points of the M vs. T curve obtained upon both heating through the FM-to-PM transition and cooling through the PM-to-FM transition. The width of the magnetic transition was estimated as the temperature span between coincident magnetothermal traces. The latent heat associated with the magnetic phase change of $AlFe_2B_2$ was determined using a NETZSCH STA 449 F3 *Jupiter* differential scanning calorimeter operated in the temperature range 170 K ≤ T ≤ 370 K at controlled heating and cooling rates of 25 K min^{-1}. For all calorimetric measurements helium was used as the carrier gas and liquid nitrogen was utilized to cool the sample below room temperature. First-order phase transitions were identified as exothermic (heating) or endothermic (cooling) peaks in the DSC data, with onset temperatures T_{onset} that define the beginning of the transition and the area encompassed by the peak representing the enthalpy of transformation ΔH. The width of the transition was quantified in the calorimeter as the intersection of the thermal trace and the linear baseline. Estimated errors for reported temperatures are ±3 K and for reported enthalpies are ~ ±10%, based on error obtained from measurement of an adamantine reference sample that demonstrates a phase transition near the magnetic transition temperature of $AlFe_2B_2$.

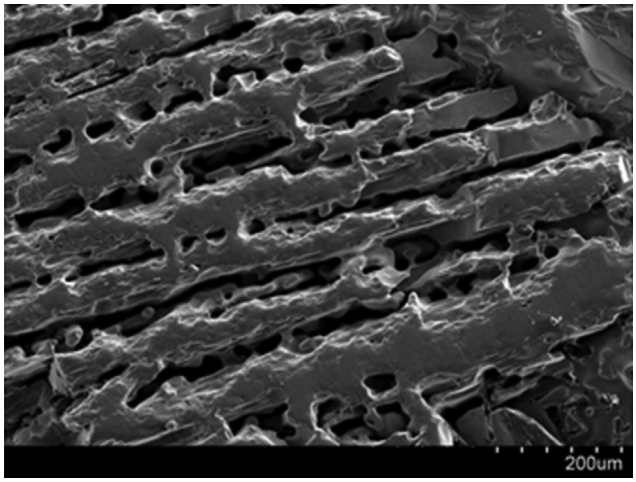

Fig. 2. SEM micrograph of annealed $AlFe_2B_2$ crystallite network synthesized by arc-melting Al, Fe and B in the molar ratio 1.5: 2: 2 showing the anisotropic microstructure and acicular formation of crystallites (20–40 micron in width and several hundred microns in length). Lighter regions correspond to $AlFe_2B_2$ and darker regions correspond to porous regions between the crystallites.

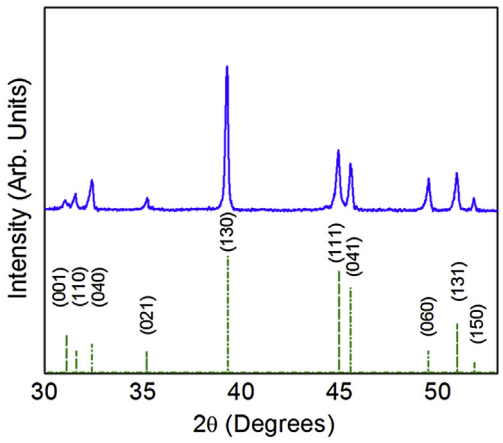

Fig. 3. X-ray powder diffraction pattern of $AlFe_2B_2$ obtained by arc-melting a mixture of elements in the ratio 1.5 Al: 2 Fe: 2B and subsequently annealing the ingot at 1000 °C for 14 days. Experimental data (blue trace) confirms the presence of $AlFe_2B_2$ with the orthorhombic $AlMn_2B_2$-type structure (green dashed lines providing reference Bragg reflections). (For interpretation of the references to colour in this figure legend, the reader is referred to the web version of this article.)

3. Experimental results

3.1. Morphological and structural attributes

Optical and scanning electron microscopy studies, including SEM-EDX investigations, indicate that the annealed slab sample microstructure consists of a network of elongated plate-like $AlFe_2B_2$ crystallites (several hundred micron in length; width = 20–40 micron), Fig. 2. X-ray diffraction measurements conducted at room temperature, shown in Fig. 3, confirm the presence of $AlFe_2B_2$ with the orthorhombic $AlMn_2B_2$-type structure with room-temperature lattice parameters $a = 2.931(1)$, $b = 11.028(4)$, $c = 2.861(1)$ Å, providing a unit cell volume of 92.5 ± 0.06 $Å^3$. While its presence is confirmed through magnetic measurement, the absence of the $Al_{13}Fe_4$ phase from the XRD data of the annealed sample is attributed to its physical location underneath the polished sample surface, in excess of the depth of the x-ray probe. As the melting temperature of $Al_{13}Fe_4$ is near 1000 °C [18], it is deduced that this phase flowed under the force of gravity,

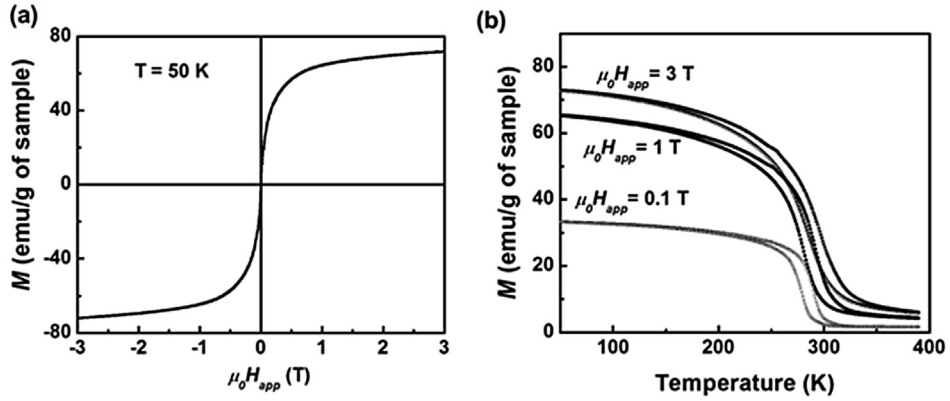

Fig. 4. Magnetic properties of bulk $AlFe_2B_2$: (a) Field-dependent magnetization ($M(H)$) curve of the $AlFe_2B_2$ system at $T = 50$ K; (b) Temperature-dependent magnetization (M(T)) curves of the $AlFe_2B_2$ sample 50 K $\leq T \leq$ 390 K at applied magnetic fields $\mu_0 H_{app} = 0.1$, 1 and 3 T.

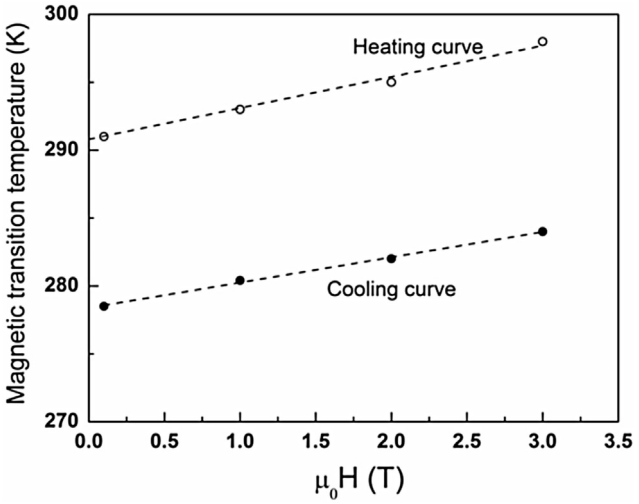

Fig. 5. Magnetic field dependence of the $AlFe_2B_2$ magnetic transition temperature featuring an increase with applied magnetic field of 2 K/T.

away from the polished sample surface, during annealing and is thus not detected with XRD measurements.

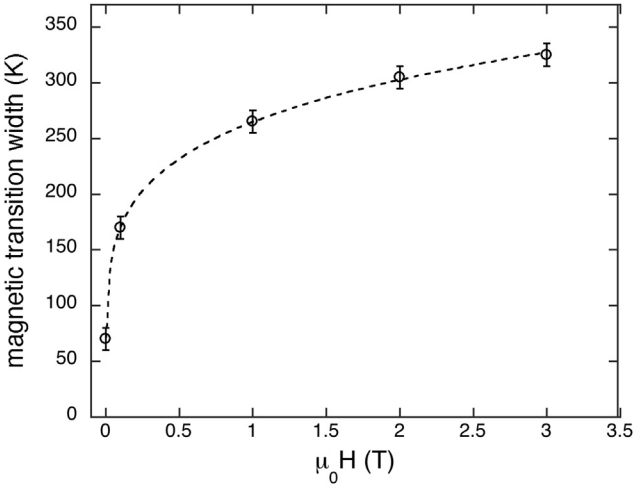

Fig. 6. Trend of magnetic transition width as a function of applied field.

3.2. Magnetic attributes

Magnetization ($M(H)$) data collected at T = 50 K, Fig. 4(a), indicate coexistence of a ferromagnetic (FM) phase of very low coercivity and a paramagnetic (PM) phase. Based on the magnetic moment of ~1.1 μ_B/Fe atom reported by El Massalami et al. the saturation magnetization M_s, of $AlFe_2B_2$ at 50 K is calculated as ~77 emu/g [16]. Utilizing this value and applying mass balance principles, the sample is determined to consist of approximately 80 wt% $AlFe_2B_2$ phase, approximately 10–15 wt% paramagnetic $Al_{13}Fe_4$ with the remainder consisting of Al(Fe) and FeB phases. Thermomagnetic data collected at an applied magnetic field of $\mu_0 H_{app} = 0.1$ T, Fig. 4(b), confirm the existence of an FM-to-PM magnetic phase transition that takes place upon heating at T = 290 K. The magnetic transition temperature increases linearly with increased applied magnetic field at a rate of $\partial T_t/\partial H = 2K/T$ (Fig. 5) with a thermal hysteresis of approximately 12 K in this sample, independent of the applied magnetic field magnitude. The breadth of the magnetic transition increases with increased applied field in a quasi-logarithmic manner, Fig. 6, with a zero-field value of approximately 60 K that approaches a maximum value of near 350 K at extrapolated infinite field.

3.3. Evolution of the crystal structure with temperature

The temperature dependence of the orthorhombic $AlFe_2B_2$ lattice parameters and of the unit cell volume are shown in Fig. 7. All three lattice parameters undergo variations upon cooling in the temperature range 200 K $\leq T \leq$ 298 K. The current data are not of sufficient resolution to assess the presence of two-phase coexistence, which is an expected feature of first-order phase transitions. The *a*-parameter, which reflects the interatomic spacing within the zig-zag Fe–B chains, exhibits a small decrease upon cooling between 280 K and 260 K, in the vicinity of the zero-field magnetic transition temperature determined upon cooling (Fig. 5). Upon further cooling the *a*-parameter remains constant in the temperature range 260–240 K and then decreases significantly at 200 K. In contrast, the *c*-parameter, representing Fe–Fe and B–B distances perpendicular, within the (*ac*) plane, to the zig-zag chains, increases in a linear fashion by 0.3% with decreasing temperature from 298 K to 200 K and shows no discontinuity in that region. The *b*-parameter that describes the distance between the planes of Fe–B chain networks, separated by the Al atoms, decreases significantly upon cooling from room temperature to 260 K, and then displays a more gradual decrease to lowest measured temperatures. Significantly, these temperature-dependent lattice parameter changes largely compensate for one another to produce

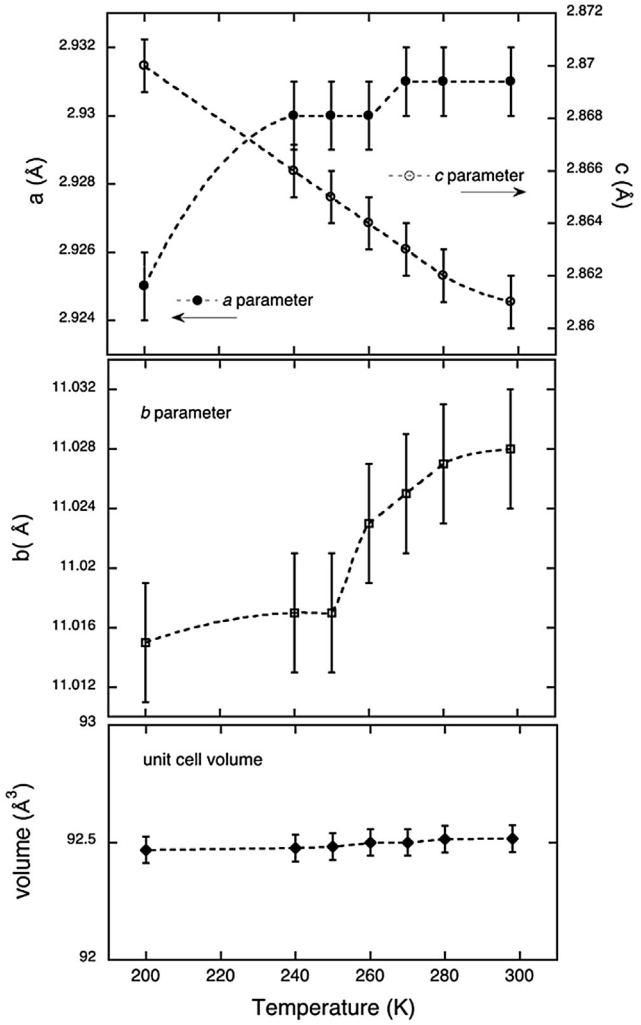

Fig. 7. Temperature-dependence of the *a*, *b*, and *c* lattice parameters and the volume of the orthorhombic $AlFe_2B_2$ unit cell.

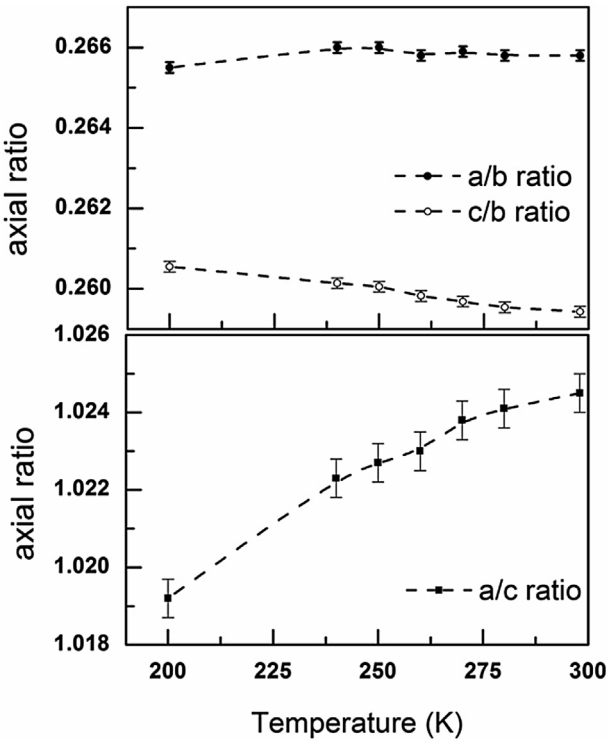

Fig. 8. Temperature-dependence of the *a*/*b*, *c*/*b*, and *a*/*c* axial ratios of the $AlFe_2B_2$ unit cell as a function of temperature.

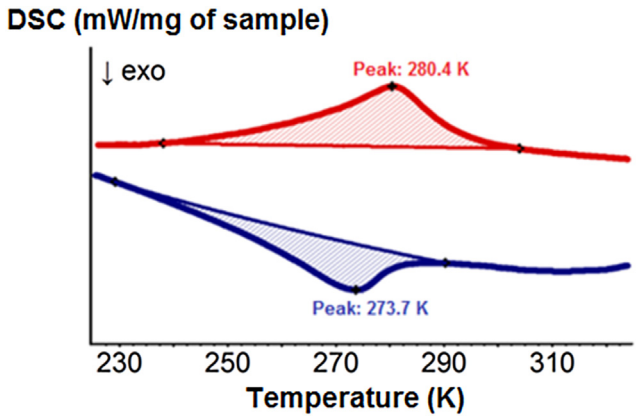

Fig. 9. Calorimetry results obtained upon heating and cooling the $AlFe_2B_2$ sample. A broad exothermic peak is noted on cooling with a peak temperature $T_{P,cool}$ = 274 K (lower panel, blue trace) and a broad endothermic peak noted on heating with a peak temperature $T_{P,heat}$ = 280 K (upper panel, red trace). (For interpretation of the references to colour in this figure legend, the reader is referred to the web version of this article.)

a negligible unit cell volume change (<0.01%) upon cooling through the magnetic transition, Fig. 7. Temperature-induced changes of the $AlFe_2B_2$ unit cell may be better visualized through examination of the axial ratios as a function of temperature, Fig. 8. A comparison of the thermal behavior of the *a*/*b* and *c*/*b* axial ratios confirms that Fe—B zig-zag chains, represented by the *a*/*b* ratio, largely maintain a constant character through the transition while the distance between the chains, illustrated by the *c*/*b* ratio, undergoes a steady contraction upon heating through the transition. The *a*/*c* ratio indicates that the distortion from square planar symmetry in the (*ac*) plane weakens to approach unity with decreasing temperature. While all three axial ratios depicted in Fig. 8 exhibit a slight dip or variation in the region 250 K < T < 270 K, in the vicinity of the magnetic transition temperature, these data are not sufficiently precise to enable definitive conclusions.

3.4. Calorimetric attributes

The calorimetric data of Fig. 9 obtained upon heating and cooling through the transition temperature confirms the existence of a reversible and reproducible peak with peak temperatures T_p~ 274 K (cooling, exothermic, lower panel) and T_p~ 280 K (heating, endothermic, upper panel). Overall, the calorimetric peaks are very broad, spanning a temperature range of 60°, which is consistent with the starting and ending points of the transition as measured by magnetometry. Within experimental error, the $AlFe_2B_2$ peak transition temperatures obtained via calorimetry are ~6 K lower than the corresponding values determined by magnetic measurement. The latent heat of the phase transformation ΔH was determined as 4.4 ± 0.4 kJ/kg, a value that is comparable with that of other magnetocaloric compounds such as $(Mn_{0.94}Cu_{0.06})As$ (ΔH = 5.76 kJ/kg) [19] and $Fe_{49}Rh_{51}$ (ΔH = 2.9 kJ/kg) [20].

4. Discussion & conclusions

All data reported here indicate that the intermetallic compound $AlFe_2B_2$ undergoes a thermodynamically first-order magnetic

Table 1
Compilation of zero-field magnetostructural transition temperatures for the $AlFe_2B_2$ sample of this study, as determined by magnetic and calorimetric probes.

Probe	Transition temperature (K)	Transition width (K)
Magnetic (VSM)	279.5 (cooling); 290.5 (heating)	60
Calorimetric (DSC)	273.7 (cooling); 280.4 (heating)	60 (cooling); 68 (heating)

phase transition that is magnetostructural in nature, but with minimal unit cell volume change through the transition. The measured room-temperature lattice parameters ($a = 2.931(1)$, $b = 11.028(4)$, $c = 2.861(1)$ Å) and the determined magnetic transition temperature are consistent with those reported in previous studies [8,11,16]. A summary of the transition temperatures and the breadth of the magnetic phase transition determined using magnetic and calorimetric probes, as described in the experimental section of this report, are provided in Table 1. The magnetic data are reported for zero-field ($T_t(\mu_0 H_{app} = 0\ T)$) behavior as extrapolated from Fig. 6.

Outside of experimental error, although the determined zero-field magnetic transition widths agree well, magnetostructural transition temperatures displayed in Table 1 do not precisely coincide. These transition temperatures reflect the temperature at which the measured parameter exhibits the most rapid change; therefore the 5–10° difference in measured transition temperatures may be attributed to different equipment sensitivities or may reflect an intrinsic difference in how the crystal and magnetic lattices of the $AlFe_2B_2$ structure are correlated through the transition. The rather large width of the magnetic phase transition may be ascribed to chemical and phase inhomogeneity, magnetic anisotropy (creating barriers to magnetization rotation), strain, or some combination of all these effects. The solid slab form and the presence of the residual Al-rich matrix phase in the sample of this study may donate "clamping" effects that are anticipated to impact the interaction between the structural and magnetic lattices, thereby influencing the nature of the magnetostructural phase transition. All of these considerations are important for contemplation of $AlFe_2B_2$-based materials as components for functional systems.

The above observations are further enriched by the unusual evolution of the lattice parameters as the sample is cooled though the magnetic transition temperature. The *a*-parameter decreases slightly but discontinuously in the region 260 K < T < 270 K, Fig. 7. Within experimental uncertainty, this is the same temperature range of the transition determined with magnetic and calorimetric probes, confirming the dominant role that intrachain Fe–B–Fe bonding plays in the magnetic transition, with shorter Fe–B–Fe bonds associated with ferromagnetic character. The negative thermal expansion of the *c*-parameter opposes the intrachain thermal expansion within the Fe–B layers of the structure. Similar to the behavior of the *a*-parameter, the increase of the *b*-parameter with increasing temperature exhibits a clear discontinuity that occurs in the temperature range 250 K < T < 260 K, which is approximately 10° lower than the analogous *a*-parameter change. There is no significant discontinuity in the unit cell volume of $AlFe_2B_2$ in this temperature range of interest. A volumetric thermal expansion coefficient of approximately 4.4×10^{-6}/K is determined for the $AlFe_2B_2$ sample studied, a value that is one order of magnitude smaller than that of aluminum (69×10^{-6}/K) [20] and only slightly larger than that of Invar (3.6×10^{-6}/K) in this temperature range [20]. This behavior is similar to that reported for the widely-studied MnFe(P,x; x = As, B, Si) system with the orthorhombic Fe_2P structure type, identified as a giant magnetocaloric material [21,22]. The structure with the specific composition of $MnFe_{0.95}P_{0.595}B_{0.075}Si_{0.33}$ has been asserted to show an exceptionally small volume change on the order of 0.05% at the magnetostructural transition temperature of 270 K [23,24], very similar to the value reported here for $AlFe_2B_2$.

In conclusion, the magnetostructural phase transition of a bulk $AlFe_2B_2$ sample was examined using a variety of structural, magnetic, and thermal probes to furnish information concerning inherent spin-lattice interactions. The Curie transition in this system exhibits thermal hysteresis between the heating and cooling magnetothermal curves and a shift in the Curie temperature as a function of applied magnetic field ($dT_c/dH = 2\ K/T$), which is accompanied by the evolution of latent heat ($\Delta H = 4.4$ J/g). Consequently, it is asserted that the magnetic transition in $AlFe_2B_2$ has a first-order thermodynamic character. In the vicinity of the magnetic transition the $AlFe_2B_2$ compound undergoes a volume-conserved change in the lattice parameters of the orthorhombic unit cell. In particular, it is noted that the lattice parameters *a* and *b* increase by 0.2% and 0.1% respectively, while *c* decreases by 0.3% upon heating the sample from its ferromagnetic state at T ~200 K to its paramagnetic state at 298 K. The Fe–B–Fe intrachain bonds of the layered $AlFe_2B_2$ structure correlate with the magnetic transition, with smaller intrachain distances favoring ferromagnetic interactions. The role of strain in the character of the magnetostructural phase transition, including the transition temperature and transition width, remains an open question that has important relevance for potential applications of this compound. In total, these results furnish insight of both fundamental and applied character concerning possible routes towards developing and tailoring the magnetofunctionality of the $AlFe_2B_2$ compound.

Acknowledgements

Research was funded by Northeastern University and by the US Army under grant W911NF-10-2-0098, subaward 15-215456-03-00.

References

[1] W. Goetzler, R. Zogg, J. Burgos, H. Hiraiwa, J. Young, Energy Savings Potential and RD & D Opportunities for Commercial Building HVAC Systems, Report submitted to U.S, Department of Energy (Energy Efficiency and Renewable Energy Building Technologies Program), September 30th, 2011.
[2] A. Chen, Thermal Energy Harvesting with Thermoelectrics for Self-powered Sensors: with Applications to Implantable Medical Devices, Body Sensor Networks and Aging in Place, Ph.D. dissertation, University of California, Berkeley, 2011.
[3] S. Fähler, U.K. Rößler, O. Kastner, J. Eckert, G. Eggeler, H. Emmerich, P. Entel, S. Müller, E. Quandt, K. Albe, Caloric effects in ferroic materials: new concepts for cooling, Adv. Eng. Mater 14 (2012) 10–19.
[4] K.J. Gschneidner, V. Pecharsky, Magnetocaloric materials, Annu. Rev. Mater. Sci. 30 (2000) 387–429.
[5] A. Kitanovski, Magnetocaloric Energy Conversion: From theory to applications, first ed., Springer, Berlin, Germany, 2015.
[6] E. Brück, O. Tegus, D.T. Cam Thanh, N.T. Trung, K.H.J. Buschow, A review on Mn-based materials for magnetic refrigeration: structure and properties, Int. J. Refrig. 31 (2008) 763–770.
[7] V. Franco, J.S. Blázquez, B. Ingale, A. Conde, The magnetocaloric effect and magnetic refrigeration near room temperature: materials and models, Annu. Rev. Mater. Res. 42 (2012) 305–342.
[8] X. Tan, P. Chai, C.M. Thompson, M. Shatruk, Magnetocaloric effect in $AlFe_2B_2$: toward magnetic refrigerants from earth-abundant elements, J. Am. Chem. Soc. 135 (2013) 9553–9557.
[9] V.K. Pecharsky, K.A. Gschneidner Jr., Magnetocaloric effect and magnetic refrigeration, J. Magn. Magn. Mater 200 (1999) 44–56.
[10] R. Barua, F. Jiménez-Villacorta, L.H. Lewis, Towards tailoring the magnetocaloric response in FeRh-based ternary compounds, J. Appl. Phys. 115 (17) (2014) 17A903.
[11] W. Jeitschko, The crystal structure of Fe_2AlB_2, Acta Crystallogr. 25 (1969)

163–165.
[12] V.H.J. Becher, K. Krogmann, E. Peisker, Uber das ternare Borid Mn_2AlB_2, Z. Anorg. Allg. Chem. 344 (1966) 140–147.
[13] P. Chai, S.A. Stoian, X. Tan, P.A. Dube, M. Shatruk, Investigation of magnetic properties and electronic structure of layered-structure borides AlT_2B_2 (T=Fe, Mn, Cr) and $AlFe_{2-x}MnxB_2$, J. Solid State Chem. 224 (2015) 52–61.
[14] L.D. Gulay, M. Wol, Cryst. Struct. R2Ni2Pb (R = Y, Sm, Gd, Tb, Dy, Ho, Er, Tm, Lu) Compd. 311 (2000) 228–233.
[15] F. Canepa, S. Cira, F. Merlo, M. Pani, C. Ferdeghini, Antiferromagnetism GdNi Cd 195 (1999) 646–650.
[16] M. ElMassalami, D.D.S. Oliveira, H. Takeya, On the ferromagnetism of $AlFe_2B_2$, J. Magn. Magn. Mater. 323 (2011) 2133–2136.
[17] G.A. Nowak, A.A. Colville, A practical interactive least-squares cell-parameter program using an electronic spreadsheet and a personal computer, Am. Min. 74 (1989) 488–490.
[18] F. Stein, M. Palm, Re-determination of transition temperatures in the Fe–Al system by differential thermal analysis, Int. J. Mater. Res. 98 (7) (2007) 580–588.
[19] A.L. Lima Sharma, S. Gama, A.A. Coelho, A. De Campos, Irreversibility in cooling and heating processes in the magnetocaloric MnAs and alloys, Appl. Phys. Lett. 93 (2008) 261910.
[20] M.P. Annaorazov, S.A. Nikitin, A.L. Tyurin, K.A. Asatryan, A.K. Dovletov, Anomalously high entropy change in FeRh alloy, J. Appl. Phys. 79 (1996) 1689–1695.
[21] William M. Haynes, David R. Lide, CRC Handbook of Chemistry and Physics: a Ready Reference Book of Chemical and Physical Data, CRC, Boca Raton, Fla, 2010.
[22] D.T. Thanh, E. Bruck, N.T. Trung, J.C.P. Klaasse, K.H.J. Byschow, Z.Q. Ou, O. Tegus, L. Caron, Structure, magnetism, and magnetocaloric properties of $MnFeP_{1-x}Si_x$ compounds, J. Appl. Phys. 103 (2008) 07B318.
[23] E. Brück, M. Ilyn, A.M. Tishin, O. Tegus, Magnetocaloric effects in $MnFeP_{1-x}As_x$-based compounds, J. Magn. Magn. Mater 290 (2005) 8–13.
[24] F. Guillou, G. Porcari, H. Yibole, N. van Dijk, E. Brück, Taming the first-order transition in giant magnetocaloric materials, Adv. Mater 26 (2014) 2671–2675.